# Experience from Two Resistivity Inversion Techniques Applied in Three Cases of Geotechnical Site Investigation

Roger Wisén[1]; Anders V. Christiansen[2]; Torleif Dahlin[3]; and Esben Auken[4]

**Abstract:** The combination of in situ geotechnical testing and continuously measured geophysical data can be a powerful tool in geotechnical site investigation. In two cases from Sweden and one case from Denmark electric resistivity surveys are used successfully in geotechnical site investigations. The main contribution of resistivity results is the possibility to interpret continuous geological models. An improved methodology combines two-dimensional (2D) smooth inversion and 2D laterally constrained inversion (2D-LCI) to significantly increase interpretability. The 2D smooth inversion has high horizontal resolution and 2D-LCI high vertical resolution. The possibility to add a priori information from, for example, drill log data to constrain the 2D-LCI increases the confidence in the inverted model and limits ambiguity. In a site investigation for a railway trench in southern Sweden a geotechnical data set is used as a priori data to increase the reliability of the inversion of the resistivity data. From this combined survey a complex Quaternary geology is described in detail. A slope stability study from south of Stockholm, Sweden, employed resistivity data together with refraction seismic and geotechnical drill log data. The result gives necessary geometrical information for the important geological units, for example for stability calculations. Both these surveys were performed with a multielectrode system. In the third case a pulled array resistivity survey was used to map the uppermost 15–20 m to estimate the distribution of the geological formations for freeway construction in Denmark. The result enables a more accurate estimate of the total freeway construction costs.

**DOI:** 10.1061/(ASCE)1090-0241(2008)134:12(1730)

**CE Database subject headings:** Site investigation; Geophysical surveys; Electrical resistivity; Measurement; Numerical models; Highway and road construction; Slope stability.

## Introduction

The adaptation of geophysical methods for engineering purposes represents an important contribution to the development of site investigation methodology (Morgenstern 2000; Stokoe et al. 2004). It is important to have a well-established conceptual geological model that serves as a framework in which other types of data can be placed (Sharp et al. 2000); most infrastructure investigations require that the conceptual models are at least two-dimensional (2D). Important as it is to achieve accurate measurements of a specific property of the ground (using, for example, auger drilling or cone penetration tests) it is in many cases difficult to create continuous models from the sparse, discrete data that come out of the detailed geotechnical investigations; however, the combination of in situ geotechnical testing and continuously measured geophysical data can achieve these important models.

We present three cases from Sweden and Denmark where resistivity measurements were used in geotechnical site investigations. In all three cases the resistivity data are measured along profiles using either the continuously vertical electrical sounding (CVES) (Dahlin 1996) or the pulled array continuous electrical sounding (PACES) (Sørensen 1996) measurement techniques. An improved methodology for interpretation, using two different inversion techniques, has been applied with success and has significantly increased the interpretability of the resistivity data. In addition to 2D smooth inversion (Oldenburg and Li 1994; Loke and Barker 1996) we use a layered and laterally constrained 2D inversion (2D-LCI) scheme (Auken and Christiansen 2004). With the 2D-LCI technique it is possible to invert the resistivity data using a layered model description utilizing inclusion of a priori data, for example, depths to layer boundaries from drill logs.

The first case is a site investigation for a railway trench in southern Sweden where an extensive geotechnical data set has been used as a priori information in the inversion of resistivity data. The second case is a slope stability investigation from south of Stockholm where resistivity imaging has been used together with refraction seismic measurements and geotechnical investigations. The third case is a site investigation for freeway construction in Denmark.

## Resistivity Measurements

Resistivity is the inverse to conductivity which describes a materials ability to conduct electric current. Since most mineral grains

[1]Rambøll Danmark A/S, Bredevej 2, DK-2830 Virum, Denmark; formerly, Engineering Geology, Lund Univ., Box 118, S-221 00 Lund, Sweden (corresponding author). E-mail: rgw@ramboll.dk

[2]Dept. of Earth Sciences, Hydrogeophysics Group, Univ. of Aarhus, Hoegh-Guldbergs Gade 2, DK-8000 Aarhus C, Denmark. E-mail: anders.vest@geo.au.dk

[3]Engineering Geology, Lund Univ., Box 118, S-221 00 Lund, Sweden. E-mail: torleif.dahlin@tg.lth.se

[4]Dept. of Earth Sciences, Hydrogeophysics Group, Univ. of Aarhus, Hoegh-Guldbergs Gade 2, DK-8000 Aarhus C, Denmark. E-mail: esben.auken@geo.au.dk

Note. Discussion open until May 1, 2009. Separate discussions must be submitted for individual papers. The manuscript for this paper was submitted for review and possible publication on November 19, 2004; approved on July 27, 2006. This paper is part of the ***Journal of Geotechnical and Geoenvironmental Engineering***, Vol. 134, No. 12, December 1, 2008. ©ASCE, ISSN 1090-0241/2008/12-1730–1742/$25.00.

**Table 1.** Summary of Geological Units, Their Properties, and Possible Resistivity Intervals at Railway Trench Site, Case 1

| Unit | Material | Comment | Expected thickness (m) | Expected resistivity (Ω m) |
|---|---|---|---|---|
| 1 | Post- or late glacial sediments, mainly sand and silt. | Situated above the groundwater surface. | 0.5–2 | 100–1,000 |
| 2 | Clay till, alternating with sand and silt layers. | — | 2–5 | 20–100 |
| 3 | Intermorainic sediments, mainly sand and silt. | The unit is found only in parts of the area. It was deposited on the lower clay till, Unit 4. | 0–3 | 50–400 |
| 4 | Clay till, silty and often containing sand. | — | 2–10 | 20–75 |
| 5 | Danian limestone. Top meters often crushed and mixed with the lower clay till, Unit 4. | Undulates slightly and rises about 10 m from east to west in the field area. The groundwater pressure level in the limestone can be found at a few meters below the ground level. | — | 100–600 |

practically are insulators the electric conduction will be electrolytic and the bulk resistivity in a geological material will be governed by the amount of pore water; water generally having several orders of magnitude lower resistivity. When clay minerals are present a large number of ions are made available through ion exchange processes, which decrease bulk resistivity. As for other physical properties, there is a considerable overlap in resistivity for different materials. There is also a great variation in resistivity for different geological materials (see examples from materials found in the case studies in Tables 1 and 2) which makes geological interpretation possible. No general correlation between lithology and resistivity exist; however, with prior knowledge on the expected geology classification is possible.

Continuous resistivity profiling to obtain a 2D image of the subsurface resistivity is a well-documented method (Griffiths and Turnbull 1985; van Overmeeren and Ritsema 1988; Griffiths and Barker 1993; Dahlin 1993, 2001), and examples of applications are: mapping of groundwater aquifers, their recharge areas, and vulnerability (Larsen et al. 2002; McGrath et al. 2002; Sørensen et al. 2005); delineation of landfill structures and leakage (Bernstone et al. 2000) and geological hazard assessment (Hack 2000; Suzuki et al. 2000). Dahlin (1996) and Pellerin (2002) give numerous examples on the application of resistivity imaging for engineering purposes. Successful examples of resistivity imaging in site investigation for construction have been presented by Dahlin et al. (1999), Hiltunen and Roth (2004), and Wisén et al. (2005). Compared to in situ geotechnical investigation, resistivity measurements are fast and cost efficient; however, since it is an indirect method, it is necessary with verification from probing measurements. The main contribution of resistivity measurements in geotechnical site investigation is that information becomes available continuously over areas or in sections and volumes. The method is very useful for early characterization of the extent of different geological units and the heterogeneity of the geology. Later in the site investigation the continuous resistivity model gives a possibility of reliable interpolation of, for example, geotechnical design parameters. Variations in resistivity within units will also reveal information about changes in porosity, clay content, water content, and grain size distribution.

**Table 2.** Summary of Resistivity of Main Sedimentary Units at Freeway Construction Site, Case 3

| Sediments | Resistivity (Ω m) |
|---|---|
| Melt water sand and gravel, unsaturated | >100 |
| Melt water sand and gravel, saturated | >60–200 |
| Clay till | 20–50 |
| Melt water clay | <30 |

### *Continuous Vertical Electrical Soundings*

In the two cases from Sweden, resistivity data were collected as CVES data with a research version of the commercially available ABEM Lund Imaging System (Dahlin 1996) consisting of a 24-bit sigma-delta analog/digital (AD) converter (Lawson Labs AD201), a current transmitter (ABEM Terrameter Booster SAS2000), a relay switch (ABEM Electrode Selector ES464), a field PC (Husky FC486), four electrode cables with 21 takeouts each at 2 m separation, and various connectors. For every measurement a controlled current (mostly 100–200 mA for the data presented here) is transmitted between the current electrodes (C1 and C2 in Fig. 2). Positive and negative current pulses are averaged in a way that filters out zero shifts and linearly varying background potentials due to, for example, electrode chargeup effects and telluric noise (Dahlin 2000), resulting in averaged potential differences that varied in the range 0.3 mV–0.9 V. The receiver (AD converter) has an input impedance of 100 GΩ, and power line grid noise is efficiently suppressed through integration of a number of complete 50 Hz periods. A number of repetitions of each measurement are normally made to control data stability. Information on the current, potential, electrode geometry, and standard deviation of data is stored in the field computer. Estimations of the measurement errors based on normal and reciprocal measurements (Parasnis 1997) have given average observation errors below 1% for the equipment, measurement setup, and type of environments studied here (Dahlin et al. 2002; Zhou and Dahlin 2003).

In the cases presented here all electrodes consist of stainless-steel spikes that are inserted a couple of decimeters into the ground surface in a straight line; through this a 2D survey is performed. The electrodes can also be placed in other ways on the ground or in boreholes, thus making it possible to perform 3D or cross-hole surveys. The first and last electrode on each cable overlaps and hence there are 81 active electrodes. A sequence of four-electrode measurements are performed on the 81 electrodes, thereafter one cable is moved from the beginning of the line to the end, thus providing 20 new electrode locations [Fig. 1(a)]. In this way the profiles are extended as long as is necessary. The measurements presented here were acquired with a Schlumberger configuration [Fig. 2(c)] with the internal electrode distance ranging from 2 to 48 m and $n$ ranging from 1 to 10; apparent resistivity for a single measurement is calculated as

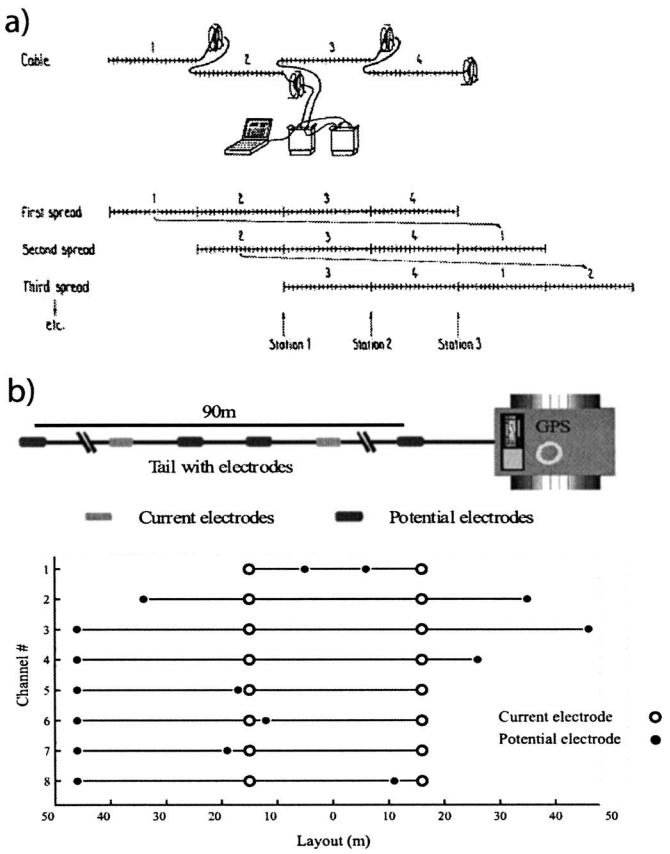


**Fig. 1.** (a) Roll-along measurement system used for acquisition of CVES data (adapted from van Overmeeren and Ritsema 1988); (b) sketch of PACES system with eight electrode configurations. Total length of electrode array is ~90 m.

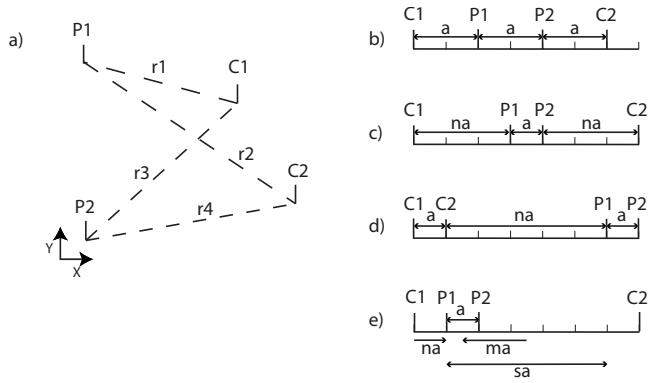


**Fig. 2.** (a) Principal of four electrode measurement setup with two potential electrodes and two current electrodes on ground; (b) Wenner array: $a$=internal electrode distance; (c) Schlumberger array: $a$=distance between potential electrodes and $na$=distance between current and potential electrodes (Note: Wenner configuration is special case of Schlumberger configuration where $n=1$); (d) dipole-dipole array: $a$=distance between electrodes in current and potential dipoles and $na$=distance between current and potential dipoles; and (e) multiple gradient array: $a$=distance between potential electrodes; $na$=distance between first current electrode and first potential electrode, $ma$=distance between midpoint of potential dipole and midpoint of current dipole and $s$=number of potential dipoles with internal distance a that can be distributed in array

$$\rho_a = K \times \frac{U}{I} (\Omega\ \mathrm{m}) \tag{1}$$

where $U$=measured potential; $I$=current; and

$$K = 2\pi \left[ \left( \frac{1}{r_1} - \frac{1}{r_2} \right) - \left( \frac{1}{r_3} - \frac{1}{r_4} \right) \right]^{-1} \tag{2}$$

=geometrical factor based on the internal positioning of the electrodes (Fig. 2).

Depth penetration depends on both array geometry and the resistivity distribution, which is not known in advance, and can be roughly estimated to be about 25–30 m. The maximum penetration depth can be increased significantly using larger electrode distances; however, this will also decrease the surface resolution. The production rate is highly dependent on terrain and measurement setup (mainly electrode distance); for the setup used here it is around 300–400 line m/day with a field crew of two persons.

### *Pulled Array Continuous Electrical Soundings*

The PACES system consists of a small tractor, equipped with processing electronics, that pulls the electrodes mounted on a tail (Sørensen 1996; Sørensen et al. 2005). The electrodes are cylindrical steel tubes with a weight of about 15 kg each. A sketch of the system and the electrode configurations is shown in Fig. 1(b).

Two electrodes with a current of 2–30 mA are maintained as sources. The current is maintained at a constant level with a constant-current generator in order to facilitate data processing. It is possible to transmit 1–30 mA using a fast operating current generator with a maximum voltage of 300 V. Processing electronics with a high input resistance of 5–10 MΩ are mounted inside the remaining steel tubes serving as potential electrodes. Analogue band-pass filtering is implemented to reduce the noise effect of slowly varying self-potential voltages of less than 1 Hz.

Electrochemical interactions between the rapidly changing soil environment and metal potential electrodes are by far the largest noise sources. The decay times are on the order of seconds. Clearly this is not an issue when using traditional metal rods, but in the case of moving electrodes the influence is severe. The noise is suppressed by applying synchronous detection techniques with a frequency of 15–25 Hz followed by robust averaging rejecting outliers.

Data collection is continuous at approximately 1.5 m/s with one full sounding saved each second. The maximum penetration depth of the system is 20–25 m. The production rate is 10–15 line km/day.

The calculation of apparent resistivity for the PACES system and the preprocessing in general is similar to that of the CVES system described above.

## Inversion Techniques

Inversion of geophysical data is most often the last step in the interpretation of a geophysical model. In contrast to the measured data, the inverted model can be interpreted directly for the physical features that it describes; however, the inverted model has limitations that are important to acknowledge. Data collection is time consuming and it is often impossible to obtain the data quality and quantity that is needed to resolve a given physical model. Due to the nature of geophysical data the geophysical model may have problems with hidden or suppressed layers, nonuniqueness, equivalence and lack of resolution in parts of the model. Hidden

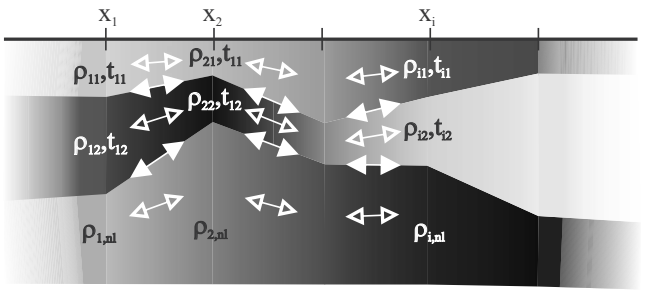


**Fig. 3.** Schematic of 2D-LCI model setup. Model is defined at number of nodes, $x$, with layer resistivities and layer thicknesses, which are interpolated to create 2D model. Open arrows indicate lateral constraints on resistivities; closed arrows lateral constraints on depths. Each model node also allows a priori constraints on resistivities, thicknesses, and depths.

or suppressed layers occur, for example, when a layer is thin or in low contrast compared to surrounding layers. Then it will not be possible to distinguish. The fact that there are an infinite number of resistivity models that fit a dataset is called nonuniqueness. When the range of model parameters is small this is not a problem; however, lack of sensitivity to some model parameters will result in high uncertainty of these and the range of possible values for the model parameter becomes large. Equivalence occurs when, for example, the thickness and resistivity of a layer can be altered and still produce the same data. High-resistivity equivalence occurs when a resistive layer is embedded between two conductive layers; then, in that case there is enough information to give the product of the resistivity and thickness, but not any of the separate parameters. If a priori data on the geometry are available this will give the additional information that is necessary to get a correct estimate of the resistivity. An example of this is given in Case 1.

The inversion algorithms of the 2D-LCI and the traditional smooth 2D inversion are not identical but share many common features. This section covers a short summary of the two algorithms with particular focus on how the inversions can be constrained to improve resolution and achieve good results. For the 2D-LCI algorithm, more details are found in Auken and Christiansen (2004). The smooth 2D inversion is described in Loke and Barker (1996).

CVES data are traditionally processed using 2D smoothness constrained inversion (Oldenburg and Li 1994; Loke and Barker 1996) that produces cell-based minimum structure 2D resistivity models. The 2D-LCI performs a parametrized, layered inversion of many datasets by tying neighboring, few-layered, 1D models together with lateral constraints on the model parameters (Auken and Christiansen 2004) as illustrated in Fig. 3. The model in the 2D-LCI is described as nodes with layer resistivities and layer thicknesses, interpolated to build a full 2D model (Fig. 3). Applying lateral constraints results in a layered and laterally smooth 2D model. Forward responses for a 2D resistivity model are calculated with a finite difference or finite-element method in the same way for both algorithms; however, for the 2D-LCI a finite difference grid is superimposed on the layered model.

The dependence of apparent resistivities on subsurface parameters is generally described as a nonlinear, differentiable forward mapping, stated as a linearized approximation by the first term of the Taylor expansion

$$\mathbf{d}_{\text{obs}} \cong \mathbf{g}(\mathbf{m}_{\text{ref}}) + \mathbf{G}(\mathbf{m}_{\text{true}} - \mathbf{m}_{\text{ref}}) + \mathbf{e}_{\text{obs}} \tag{3}$$

where $\mathbf{g}$=nonlinear mapping of the model to the data space; and $\mathbf{d}_{\text{obs}}$=observed data (apparent resistivities) with the corresponding error $\mathbf{e}$. For 2D-LCI the model vector, $\mathbf{m}$, contains layer resistivities and layer thicknesses

$$\mathbf{m} = [\rho_1, T_1, \rho_2, T_2, \cdots, \rho_n, T_n] \tag{4a}$$

while for 2D smooth inversion, with a cell-based resistivity model, it contains the cell resistivities

$$\mathbf{m} = [\rho_1, \rho_2, \cdots, \rho_n] \tag{4b}$$

The true model, $\mathbf{m}_{\text{true}}$, has to be sufficiently close to some arbitrary reference model $\mathbf{m}_{\text{ref}}$ for the linear approximation to be valid. In short, we write

$$\mathbf{G}\delta\mathbf{m}_{\text{true}} = \delta\mathbf{d}_{\text{obs}} + \mathbf{e}_{\text{obs}} \tag{5}$$

where $\delta\mathbf{d}_{\text{obs}} = (\mathbf{d}_{\text{obs}} - \mathbf{g}(\mathbf{m}_{\text{ref}}))$ and $\delta\mathbf{m}_{\text{true}} = \mathbf{m}_{\text{true}} - \mathbf{m}_{\text{ref}}$. The Jacobian matrix, $\mathbf{G}$, contains the partial derivatives of the mapping

$$G_{st} = \frac{\partial d_s}{\partial m_t} = \frac{\partial \log(d_s)}{\partial \log(m_t)} = \frac{m_t}{d_s}\frac{\partial d_s}{\partial m_t} \tag{6}$$

The logarithm ensures positivity of the data and the model parameters (Johansen 1977; Ward and Hohmann 1987).

### Constraints in 2D-LCI

In combination with the observed data the LCI method includes information on the lateral constraints and a priori information. These information sources can be thought of as *user data*, i.e., *data* added by the user containing information on either geologic variability (constraints) or known model parameters (a priori *data*). Hence, they are added to the inversion scheme similar to the observed data, linked to the true model.

The constraints are connected to the true model by

$$\mathbf{R}\delta\mathbf{m}_{\text{true}} = \delta\mathbf{r} + \mathbf{e}_r \tag{7}$$

where $\mathbf{e}_r$=error on the constraints with 0 as the expected value, and $\delta\mathbf{r} = -\mathbf{R}\mathbf{m}_{\text{ref}}$ claims identity between the parameters tied by constraints in the roughening matrix $\mathbf{R}$, containing $1s$ and $-1s$ for the constrained parameters and 0 in all other places. The variance, or strength of the constraints, is described by the covariance matrix $\mathbf{C}_R$. In this approach we only operate with lateral constraints although vertical constraints can be used as well.

Prior information on parameters (resistivities, thicknesses, and depths) is similarly included as an extra dataset, $\mathbf{m}_{\text{prior}}$, (Jackson 1979)

$$\mathbf{P}\delta\mathbf{m}_{\text{true}} = \delta\mathbf{m}_{\text{prior}} + \mathbf{e}_{\text{prior}} \tag{8}$$

where $\delta\mathbf{m}_{\text{prior}} = \mathbf{m}_{\text{prior}} - \mathbf{m}_{\text{ref}}$ and $\mathbf{e}_{\text{prior}}$=error on the prior model with 0 as the expected value; and $\mathbf{P}$=identity matrix claiming identity between the prior value and the model value. The variance in the prior model is described in the covariance matrix $\mathbf{C}_{\text{prior}}$.

By joining Eqs. (5), (7), and (8) we write the inversion problem as

$$\begin{bmatrix} \mathbf{G} \\ \mathbf{R} \\ \mathbf{P} \end{bmatrix} \cdot \delta\mathbf{m}_{\text{true}} = \begin{bmatrix} \delta\mathbf{d}_{\text{obs}} \\ \delta\mathbf{r} \\ \delta\mathbf{m}_{\text{true}} \end{bmatrix} + \begin{bmatrix} \mathbf{e}_{\text{obs}} \\ \mathbf{e}_r \\ \mathbf{e}_{\text{prior}} \end{bmatrix} \tag{9}$$

or more compactly

$$\mathbf{G}' \cdot \delta\mathbf{m}_{\text{true}} = \delta\mathbf{d}' + \mathbf{e}' \tag{10}$$

The covariance matrix for the joint observation error, $e'$, becomes

$$\mathbf{C}' = \begin{bmatrix} \mathbf{C}_{\text{obs}} & \underline{\underline{0}} & \\ & \mathbf{C}_R & \\ \underline{\underline{0}} & & \mathbf{C}_{\text{prior}} \end{bmatrix} \tag{11}$$

### Inversion Solutions

The model estimate of the 2D-LCI as the model update of the $n$th iteration

$$\delta\mathbf{m}_{n+1} = (\mathbf{G}_n'^T\mathbf{C}'^{-1}\mathbf{G}_n' + \lambda_n\mathbf{I})^{-1}\mathbf{G}_n'^T\mathbf{C}'^{-1}\delta\mathbf{d}_n' \tag{12}$$

where $\lambda$=damping parameter, minimizes

$$Q_{\text{2D-LCI}} = \left(\frac{1}{N+A+M}[(\delta\mathbf{d}_n'^T\mathbf{C}'^{-1}\delta\mathbf{d}_n')]\right)^{1/2} \tag{13}$$

where $N$=number of data; $A$=number of constraints; and $M$ =number of model parameters. In Eq. (12) $\mathbf{I}$=identity matrix; and $\lambda$=Marquart damping (Marquart 1963). In each iteration $\lambda$ is chosen to give a satisfactory improvement of the quality measure.

All data sets are inverted simultaneously, minimizing a common objective function. The lateral constraints, the a priori information, and the data are all part of the inversion. Consequently, the output models form a balance between the constraints, the a priori information, the physics, and the data. Model parameters with little influence on the data will be controlled by the constraints and/or a priori data and vice versa. Due to the lateral constraints, information from one model will spread to neighboring models.

In a similar fashion the model update at the $n$th iteration for the 2D smooth inversion

$$\delta\mathbf{m}_{n+1} = (\mathbf{G}_n^T\mathbf{W}_d\mathbf{G}_n + \lambda_n\mathbf{F}_R)^{-1}(\mathbf{G}_n^T\mathbf{W}_d\delta\mathbf{d}_n - \lambda_n\mathbf{F}_R) \tag{14}$$

minimizes

$$Q_{\text{smooth,2D}} = \left(\frac{1}{N}[(\delta\mathbf{d}_{\text{obs}}^T\mathbf{W}_d\delta\mathbf{d}_{\text{obs}})]\right)^{1/2} \tag{15}$$

where $\mathbf{W}_d$=weighting matrix for different elements of the data misfit ($C_{\text{obs}}$ in the 2D-LCI) and

$$\mathbf{F}_R = \alpha_x\mathbf{R}_x^T\mathbf{R}_x + \alpha_z\mathbf{R}_z^T\mathbf{R}_z \tag{16}$$

where $\mathbf{R}_x$ and $\mathbf{R}_z$=roughness matrices ($\mathbf{R}$ in the 2D-LCI) that claim identity between neighboring model cells resistivity in the $x$ and $z$ direction and $\alpha_x$ and $\alpha_z$=relative weight to these filters. The use of these filters can enhance vertical or horizontal features. In the laterally smooth geological setting in Case 1 $\alpha_x$ was set four times stronger then $\alpha_z$.

In general the final result depends mainly on $C'$ in 2D-LCI and $W_d$, $\alpha_x$, and $\alpha_z$ in 2D smooth inversion.

### Sensitivity Analysis of Model Parameters in 2D-LCI

Because the 2D-LCI is a truly over determined problem with more data than there are model parameters, we can produce a sensitivity analysis of model parameters to assess the resolution of the inverted model. It is not possible to do a model parameter analysis for an underdetermined problem as the smooth 2D inversion. The parameter sensitivity analysis of the final model is the linearized approximation of the covariance of the estimation error, $\mathbf{C}_{\text{est}}$ (Tarantola and Valette 1982)

$$\mathbf{C}_{\text{est}} = (\mathbf{G}'^T\mathbf{C}'\mathbf{G}')^{-1} \tag{17}$$

Standard deviations on model parameters are calculated as the square root of the diagonal elements in $C_{\text{est}}$. For slightly nonlinear problems, this is a good approximation. Because the model parameters are represented as logarithms, the analysis gives a standard deviation factor (STDF) on the parameter $m_s$ that is defined by

$$\text{STDF}(m_s) = \exp(\sqrt{C_{\text{est,ss}}}) \tag{18}$$

Thus, the theoretical case of perfect resolution has a STDF=1; a factor of STDF=1.1 is approximately equivalent to an error of 10%. Well-resolved parameters have a STDF$<$1.2, moderately resolved parameters fall within 1.2$<$STDF$<$1.5, poorly resolved parameters 1.5$<$STDF$<$2, and unresolved parameters have a STDF$>$2.

## Case 1—Construction of Railway Trench in Southern Sweden

In 1997 a parliamentary decision was made to build the Malmoe City Tunnel, named the City Tunnel Project (CTP), to improve connections between the main Swedish railway system and a combined bridge and tunnel connecting Sweden with Denmark. The construction of CTP, consisting of 17 km of railway, began in 2004 and is expected to be completed in 2010 at a cost of about 975 million euros. Resistivity measurements were made for the connection outside Malmoe through the town of Lockarp where a railway trench of about 2 km length and 10 m depth will be excavated. The reference data from almost 50 auger and a few core and hammer drill logs are used for material classifications. The locations of boreholes are shown in Fig. 4. Most of the auger and all the core and hammer drilling were performed before acquisition of the resistivity data.

### Geology

The sedimentary geological environment consists of Quaternary deposits underlain by the Danian limestone. Based on geotechnical and geophysical investigations (Danish Geotechnical Institute 1999) a geological and hydrogeological conceptual model was created and the different geological units were assigned resistivity values. Five units as described in Table 1 were identified. Since the material contains a significant amount of clay there is no detectable groundwater table. The pressure level of the groundwater in the limestone is found a few meters below the ground level.

The possibility of a large hydraulic conductivity in the intermorainic sediments and the limestone makes the groundwater situation an important issue for environmental review, design, and construction; hence, the main aim of this investigation was to determine the depth to limestone as well as layering and extent of the different soil types. Resistivity imaging was a natural choice for continuous mapping to identify areas with geological risks because the resistivity contrast between the different geological units is high.

### Resistivity Imaging

During the summer of 2000 approximately 3 km of CVES resistivity measurements were collected (Fig. 4). In the 2D smooth inversion the horizontal smoothness constraints were set four

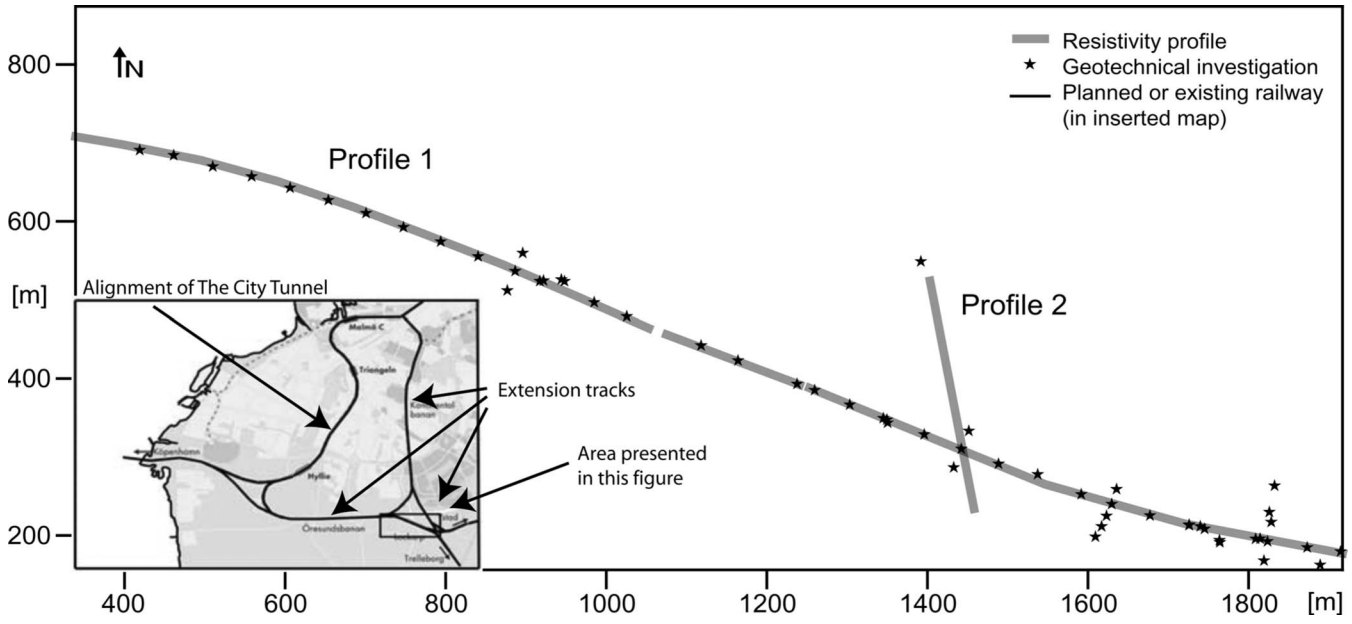


**Fig. 4.** Location map of City Tunnel Project showing CVES profile lines and locations of boreholes

times stronger than the vertical, promoting horizontally elongated features. For the 2D-LCI a five layer model was used. The model distance along the profiles is 4 m and the lateral constraints were 0.12 for all model parameters except for the depth to layer five that was set to 0.06 since this parameter, which correspond to the depth to the limestone surface, is expected to vary less. The lateral constraints in 2D-LCI force the model to become somewhat horizontally smeared, and therefore the result from the 2D smooth inversion is preferred for interpretation of vertical structures.

Apparent resistivity data, inverted models, and model parameter analysis of 2D-LCI models from Profiles 1 and 2 are shown in Figs. 5 and 6, respectively. Profile 1 follows the planned position of the railway trench and Profile 2 is roughly perpendicular crossing at coordinate 1,178 m. Profile 1 contains about 11,000 apparent resistivity data and Profile 2 contains about 3,500 apparent resistivity data. A resistivity model with five layers agrees with the expected geological and geophysical model: the high-resistivity features in the top of the profile represent post- or late-glacial sediments; the next thick, low-resistivity layer represents the two clay tills; the high-resistivity layer, sometimes present within this low-resistivity layer, is interpreted as intermorainic sediments dividing the two clay tills; and the high-resistivity bottom layer is interpreted as limestone.

The overall standard deviation of the residual error between measured data and model response is less than 2% for inversion results from the 2D smooth inversion and between 2 and 4% for the 2D-LCI. For individual data sets it can be as low as 0.3%, indicating high-quality data and a satisfying model fit. The STDF are found in Figs. 5(d) and 6(d).

### *Discussion*

The 2D smooth resistivity models in Figs. 5(e) and 6(e) show some abrupt, lateral resistivity changes, such as at profile coordinate 1,100–1,200 m in Profile 1. Because of the smoothness constraint, it is difficult to detect sharp-boundary interfaces and determine layer depths. The presence of high resistivities in Layer 3, due to the presence of intermorainic sediment, seems to cause depressions in the depth to and resistivity of Layer 5, the limestone. This originates from high-resistive equivalence in Layer 3 and provides a probable explanation as to why the depth to resistivity Layer 5 does not always agree with the depth to the limestone as found in the drill logs. From the 2D smooth resistivity models it is possible to determine the horizontal extent and depth to intermorainic sediment; however, it is not possible to define the boundaries for the bottom of the intermorainic sediment and the top of the limestone.

The 2D-LCI models in Figs. 5(b) and 6(b) clearly describe the horizontal layer interfaces of the different geological units. A priori data consisting of layer boundaries as defined by drill log data were added with a 12% standard deviation. The addition of a priori data solves ambiguity in the model and gives the resistivity model better correlation to the lithological interfaces; in addition there is very little or no increase in the data misfit. The STDF show that resistivities and depths are almost always resolved or well resolved. Inclusion of a priori data in the inversion is especially important to resolve high-resistivity equivalence. An example of this can be seen in profile coordinate 1,000–1,360 m in Profile 1 where there is a significant difference in the thickness and resistivity of layer three compared to the model from 2D smooth inversion. Although the changes of the resistivity model geometry are often small, resistivity estimates can change significantly. This effect can be seen for Layer 3 throughout most of both Profiles 1 and 2. For example, results from 2D smooth inversion show no evidence of high resistive intermorainic sediment in position 975–1,100 m in Profile 1 while in the result from 2D-LCI the resistivity of this layer is clearly higher than the resistivity of the clay tills.

From the geophysical investigations we conclude that there exists one large structure of intermorainic sediments between coordinates 1,100 and 1,200 m on Profile 1, which can also be seen around coordinate 0 m on Profile 2. A few smaller units of intermorainic sediments are also present. The limestone appears to rise about 10 m from east to west in Profile 1. While the 2D-LCI models show good correlation to lithological interfaces, the 2D smooth inversion models show high horizontal resolution. The

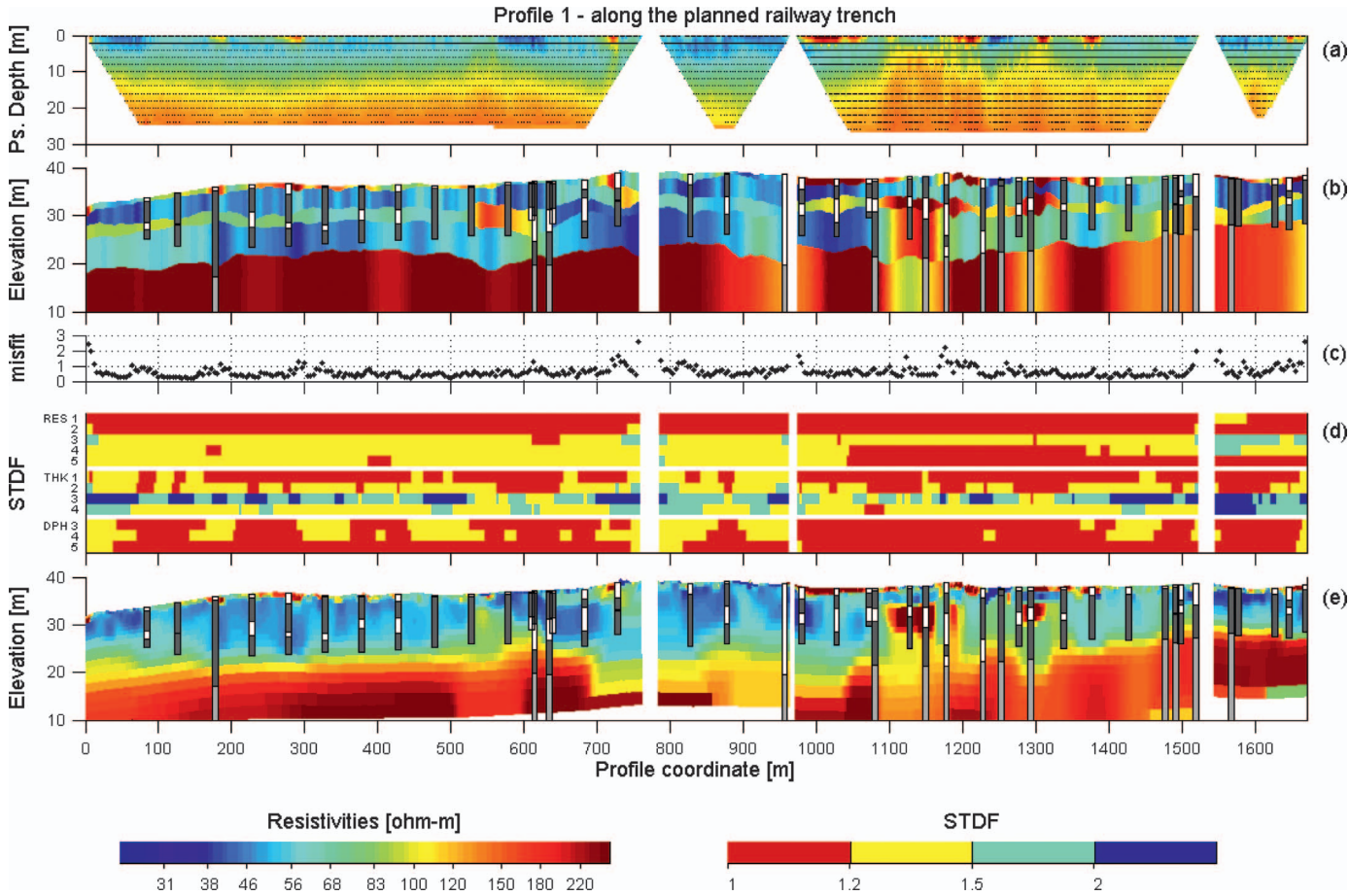


**Fig. 5.** (Color) (a) Apparent resistivity pseudosection for Profile 1, Case 1, which follows planned position of railway trench; (b) resistivity model from 2D-LCI using lithological information from drill log data as a priori data in inversion; (c) normalized residual errors (1 corresponding to error of 5%); (d) standard deviation factors (STDF) of model parameters; and (e) resistivity model from 2D smooth inversion. Sounding distance is 2 m. Data from auger and core drilling are used to differentiate mainly between clay-till (dark grey), various other sediments (intermorainic and postglacial) (white), and limestone (light gray).

combination of these two models makes a good basis for detailed geological interpretation that is not possible using only drill log data.

## Case 2—Slope Stability Investigation in Central Sweden

Following a slope failure in May 1997 a 200 by 60 $m^2$ area of clay deposits slid into the Trosa River Valley, in Vagnhärad south of Stockholm, Sweden. As a consequence there was severe damage to residential houses and infrastructure, as shown in Fig. 7. The slope failure was caused by an increase of the pore-water pressure in the clay, due to increased water pressure in the sand and silt till below the clay. Many geotechnical tests and soundings were performed in the area in order to investigate properties of the clay, but no reliable information about the surface level of the bedrock was obtained (since this was not the scope of those investigations).

In a project, funded by the Swedish Rescue Agency, Engineering Geology at Lund University, and the Swedish Geotechnical Institute, the applicability of geophysical methods for slope stability investigations was evaluated. The main goal of the geophysical surveys was to determine the geometry of the bedrock and sediments along the valley slopes, since geometry is one important property in stability calculations. The report from this project (Dahlin 2001, Swedish Geotechnical Institute, Rep. No. 62) shows that combining CVES resistivity imaging and refraction seismic surveying is a successful approach. Fig. 8 shows the position of the river, roads, remaining houses, and geophysical survey profile lines.

### *Geology*

The geological environment consists of a crystalline bedrock valley filled with mainly varved, glacial clay. Gradual erosion in and around the Trosa River, which runs through the valley, and small landslides in the river, have reduced the thickness of the clay deposits and increased the steepness of the valley slopes. The geological model consists of the following four units:

1. A surficial layer of fill material from human activities. This layer is generally above the groundwater level;
2. Several meters of clay. Geotechnical investigations found layer thicknesses of up to 14 m. The sediments are thin at the top of the valley walls and increase in thickness toward the bottom of the valley;
3. Sand and silt till with a thickness up to a few meters. This unit is sometimes found under the clay; when present this layer acts as a confined aquifer to which water infiltrates uphill; and

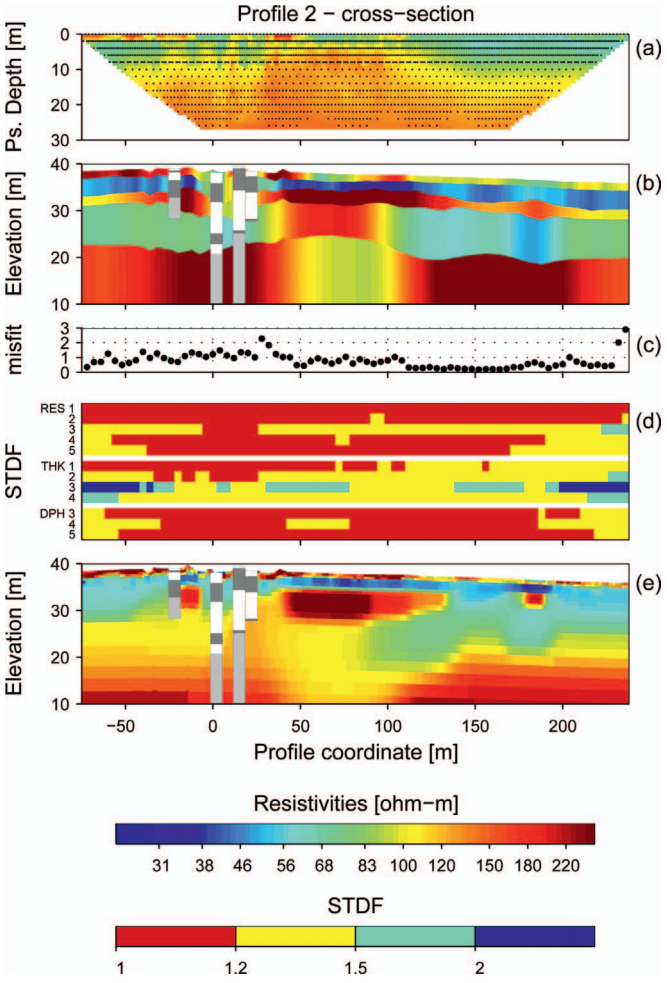


**Fig. 6.** (Color) (a) Apparent resistivity pseudosection for Profile 2, Case 1, which crosses Profile 1 at coordinate 1,178 m; (b) resistivity model from 2D-LCI using lithological information from drill log data as a priori data in inversion; (c) normalized residual errors (1 corresponding to a error of 5%); (d) standard deviation factors (STDF) of model parameters; and (e) resistivity model from 2D smooth inversion

**Fig. 7.** Photograph of residential area in Vagnhärad after slope failure within Trosa River Valley in 1997 (photographer: Jan Lindgren, Swedish Geotechnical Institute)

4. Crystalline bedrock.

As part of the geotechnical investigation, data were acquired to define properties of the clay. The depth to bedrock was not determined at all or not determined with sufficient accuracy; therefore, this information is used only as an indication of the absolute minimum depth to bedrock in the interpretation of the resistivity models. There is no detectable groundwater table in the clay. Because the aquifer confined between the bedrock and the clay reaches levels that are higher than the ground surface in parts of the field area the water below the clay can be artesian.

### Seismic Refraction Surveys

About 550 m of seismic refraction profiling was performed with a 24-channel seismograph, employing 10 Hz vertical geophones at a distance of 2 m, and an explosive source. We identify three layers in the velocity model (Fig. 9): The first layer is up to 3 m thick with velocities between 330 and 950 m/s; the second layer has a thickness between 5 and 17 m and velocities between 1,040 and 1,700 m/s; and the third layer has velocities between 3,900 and 5,100 m/s. The top layer has mostly low velocities corresponding to dry soil material, which is most likely the fill material. Velocities of the second layer indicate saturated clay and/or sand and silt till. These units are not possible to differentiate in the refraction seismic velocity model. The third layer has high velocities corresponding to the bedrock.

### Resistivity Imaging

Apparent resistivity data, inverted models, and model parameter analysis, for Profiles 1, 3, and 5 are shown in Figs. 10–12, respectively. The residual errors after inversion are quite low, between 1 and 3%. Four layers were used for the 2D-LCI. The model distance along the profiles is 4 m and the lateral constraints were 0.12 for all model parameters. In all profiles three resistivity units are clearly defined in the models resulting from the 2D-LCI without a priori data (b) and the 2D smooth inversion (h): a thin, high-resistivity layer in the top of the section; a low-resistivity layer with a thickness between 0 and 10 m; and a high-resistivity layer in the bottom. The high-resistivity layer in the top corresponds to dry fill material; the low-resistivity layer is interpreted as clay; and the high-resistivity values in the bottom of the sections correspond to both the sand and silt till and the bedrock. In these resistivity models it is not possible to clearly separate the sand and silt till and the bedrock. The STDF are found in Figs. 10, 11, and 12(d and g).

A priori data consisting of the depth to the seismic bedrock refractors was included in the inversion with 10% standard deviation on the depth values. This uncertainty of the seismic data is a rough guess but it will give a rather soft constraint and allow the resistivity data to set a different geometry in case the seismic and resistivity data disagree. The result from 2D-LCI with this a priori data clearly gives four resistivity units. In some positions, for example, along profile coordinates 125–150 m in Fig. 10(e), a fourth layer has intermediate values between the low-resistivity layer and the high-resistivity bottom layer, and is interpreted as sand and silt till.

### Discussion

The thickness and resistivity of Layer 3 are poorly resolved. In the 2D smooth inversion models [Figs. 10(d), 11(d), and 12(d)] this layer is apparent as a transition from low to high resistivity.

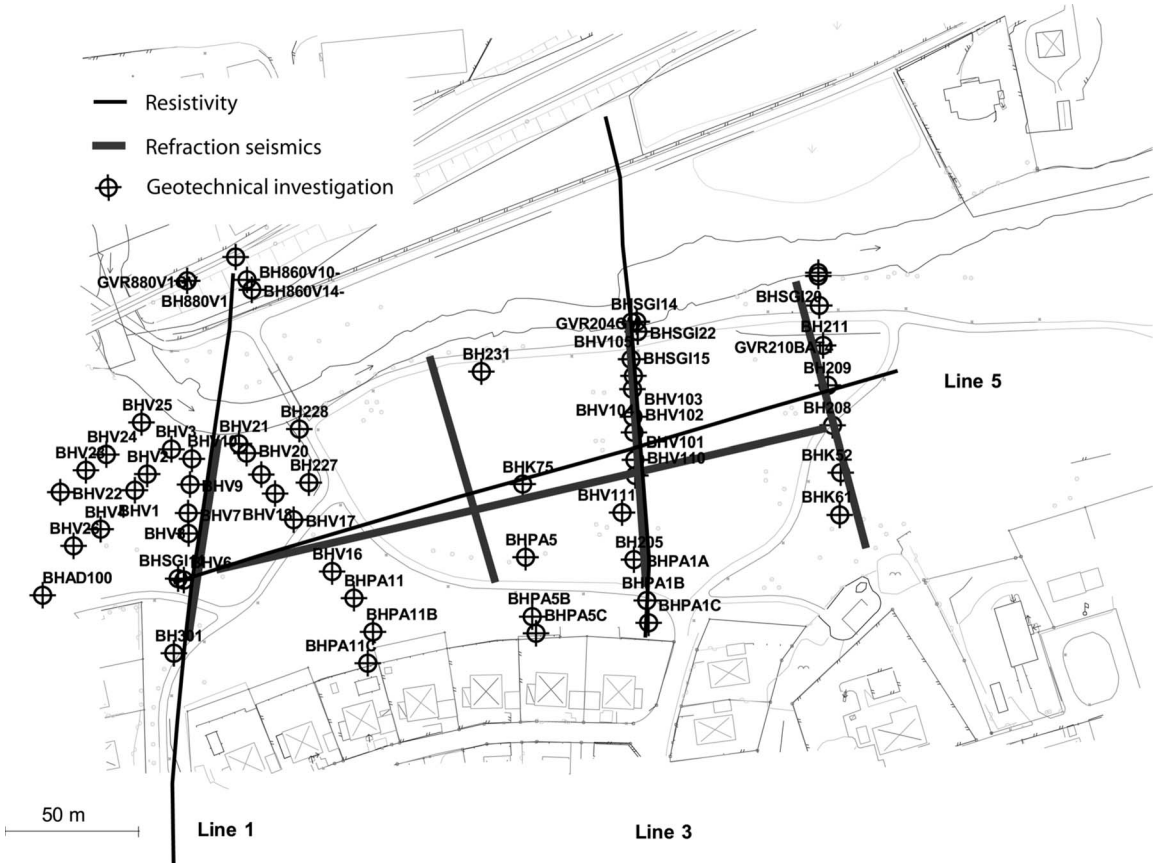


**Fig. 8.** Detailed map of investigated area showing location of geophysical survey profile lines

In the 2D-LCI without a priori data [Figs. 10(b), 11(b), and 12(b)] this layer is generally thin and has a resistivity that is similar to the low-resistive second layer. When the seismic refraction model is used as a priori data the thickness of Layer 3 changes completely and follows that of the seismic model. With a change in thickness, the resistivity of Layers 3 and 4 also change. There are clearly equivalence problems in the third layer. Without a priori data the resistivity of and depth to the third layer is unresolved while it generally becomes better resolved when a priori data are included. In some cases it is, however, shifted to solutions where the sensitivity of the data is lower and it can then be less resolved.

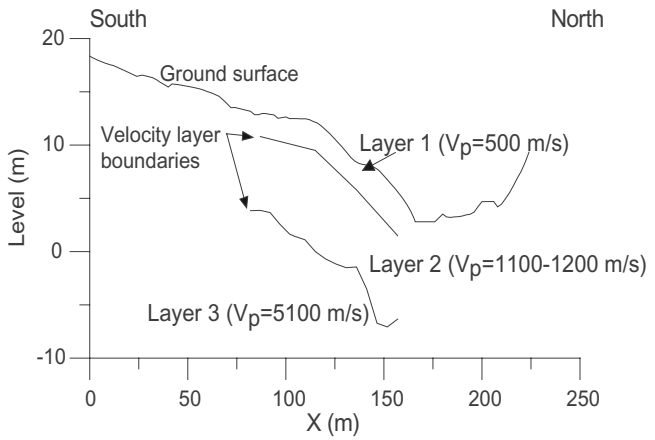


**Fig. 9.** Three-layer velocity model interpreted from seismic refraction data along Profile 1

The data misfit does not increase when a priori data are used and hence the two different models are equally likely.

The geometry of the clay, the sand, and silt till, and the bedrock surface can be derived from these geophysical models. From the combined analysis of resistivity and seismic data, the thickness of the important third layer can be quantified. These results can also be achieved from a combined interpretation of the models from 2D smooth inversion and refraction seismic; however, there is an additional benefit from inversion with the seismic data as a priori data in the knowledge that the two resistivity models (with and without a priori data) are equally likely. It is important to recognize that the depth to the bottom of this layer in both cases is resolved with the seismic data. For the combined inversion the certainty of the resistivity model depends on the certainty of the seismic model. Using the seismic model as a priori data for the resistivity imaging, it is possible to delineate the important third layer of sand and silt till and to estimate its resistivity. These results give necessary geometrical information about the geological units, for example, for stability calculations.

## Case 3—Freeway Construction in Denmark

The last case is the application of the PACES method for estimating the absolute amounts of sand relative to clay sediments in the upper 15–20 m for construction of a freeway in Denmark. A substantial cost for freeway and highway construction is related to road foundation and removal of excess material. It is important that this material is recycled locally to bring down costs; if it cannot be used locally, costly removal is necessary. For example

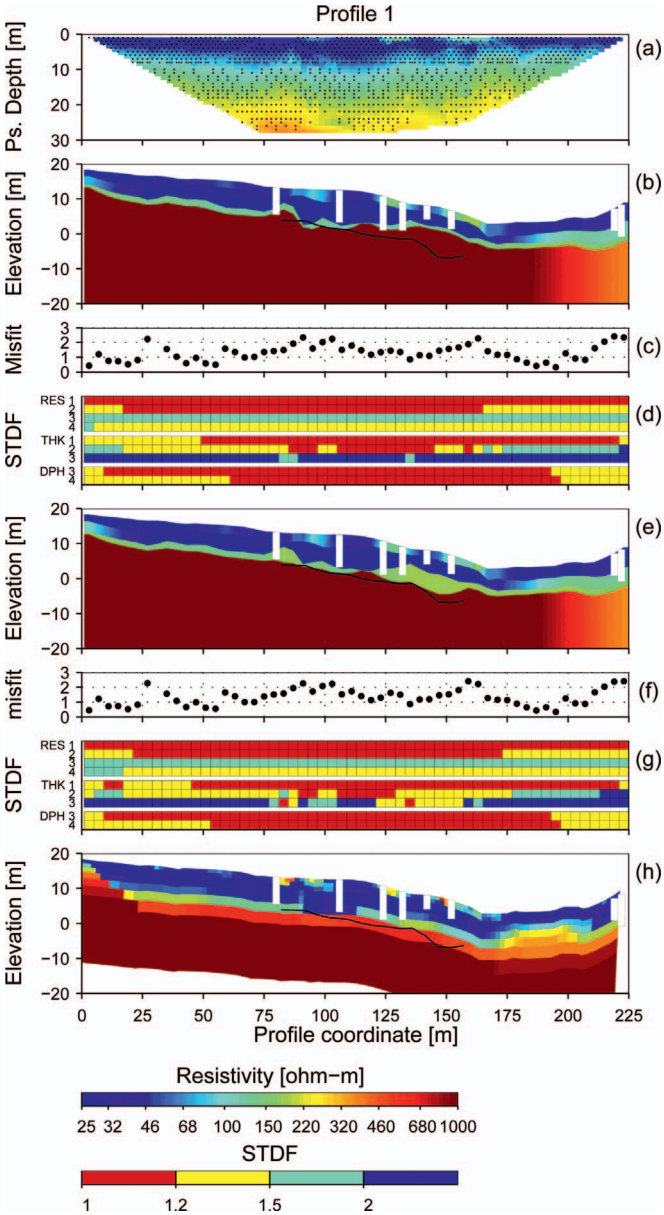


**Fig. 10.** (Color) (a) Apparent resistivity pseudosection for Profile 1, Case 2; (b) resistivity models from 2D-LCI with normalized residual errors [1 corresponding to error of 5% in (c) and standard deviation factors (STDF) of model parameters in (d)]; (e) resistivity model from 2D-LCI using layer interfaces from refraction seismic model as a priori data with normalized residual errors [1 corresponding to error of 5% in (f) and standard deviation factors (STDF) of model parameters in (g)]; and (h) resistivity model from 2D smooth inversion

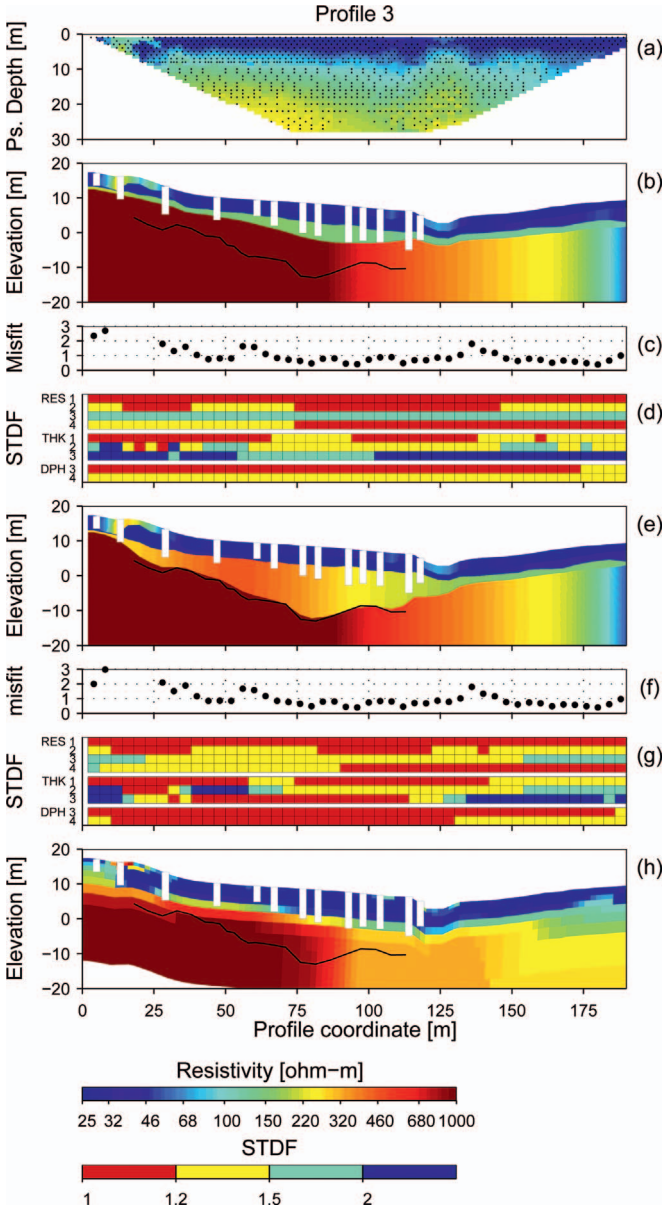


**Fig. 11.** (Color) (a) Apparent resistivity pseudosection for Profile 3, Case 2; (b) resistivity models from 2D-LCI with normalized residual errors [1 corresponding to error of 5% in (c) and standard deviation factors (STDF) of model parameters in (d)]; (e) resistivity model from 2D-LCI using layer interfaces from refraction seismic model as a priori data with normalized residual errors [1 corresponding to error of 5% in (f) and standard deviation factors (STDF) of model parameters in (g)]; and (h) resistivity model from 2D smooth inversion. Sounding distance is 2 m. Depth penetration data from shallow geotechnical probing (white) indicate only maximum possible level of bedrock surface.

excess material is the result from a situation such as when a road intersects a hill. Sand and gravel are ideal for fill and foundation, sandy clays, silts and tills can be used to some extent, whereas very clayey material has only limited or no use at all. If no sandy sediments are available locally, fill has to be transported from elsewhere, which is costly; hence, a detailed knowledge of the distribution of different materials in the upper 10–20 m is highly desirable.

Shallow holes were drilled and a PACES survey performed near the city of Herning in central Jutland (see Fig. 13) as part of the planning phase of a new freeway connecting Herning with Aarhus. The total length of the freeway is about 70 km; 35 km was opened in 2003 at a total construction cost of approximately 800 million Euro. The PACES profile follows the centerline of the freeway transect.

### *Geology*

The sedimentary geological environment consists of Quaternary deposits to large depths (more than 70 m). The base for the Quaternary deposits is dense Tertiary clays, but these are well below

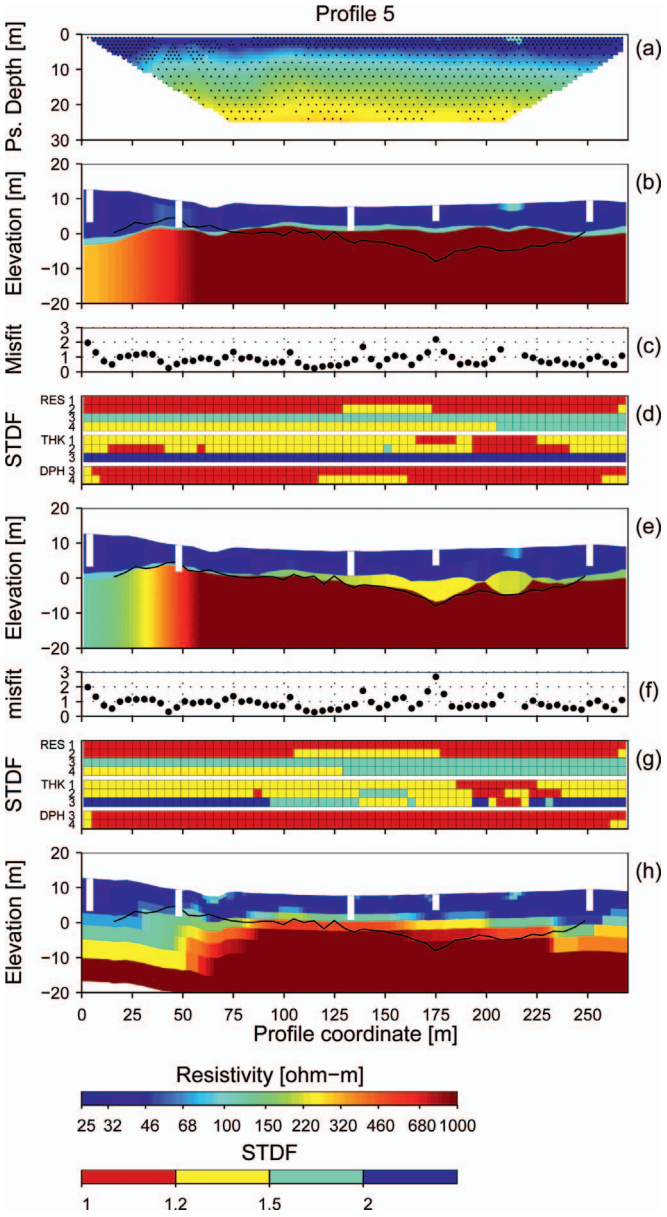


**Fig. 12.** (Color) (a) Apparent resistivity pseudosection for Profile 5, Case 2; (b) resistivity models from 2D-LCI with normalized residual errors [1 corresponding to error of 5% in (c) and standard deviation factors (STDF) of model parameters in (d)]; (e) resistivity model from 2D-LCI using layer interfaces from refraction seismic model as a priori data with normalized residual errors [1 corresponding to error of 5% in (f) and standard deviation factors (STDF) of model parameters in (g)]; and (h) resistivity model from 2D smooth inversion

the investigation depth of this survey. The Quaternary deposits consist primarily of glacio-lacustrine clays, tills and melt water sand, and gravel. The tills can be anything from very sandy to very clayey. Generally, the Quaternary deposits are structurally complex and all of the lithologies mentioned above can appear over a short range.

Auger drilling was performed at regular intervals along the freeway transect, covering the entire width of the construction site to enable mapping of the spatial variability and complexity of the geological units. The data are used to describe the geotechnical parameters, but they also give an overview of the subsurface sediments. For comparison with the PACES profiles the lithological

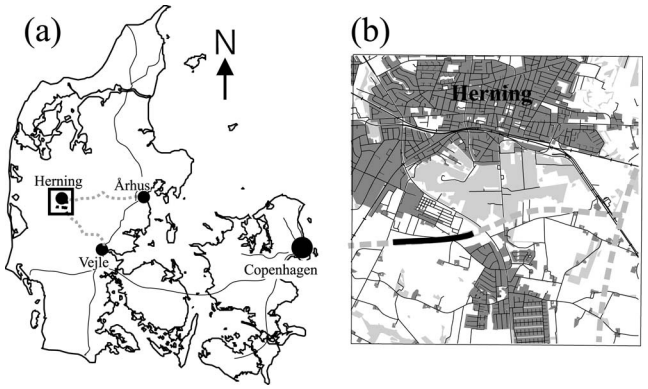


**Fig. 13.** (a) Location of Herning with planned freeway connecting Herning with Aarhus, depicted by dotted line. Many existing freeways are indicated with thin, solid line. (b) Detailed map of site with prospected freeway indicated by dashed gray line. Solid black line marks location of presented PACES profile.

descriptions are simplified to the major units, distinguishing mainly sandy and clay-rich sediments. A summary of the resistivity values for the predominant sediments is found in Table 2.

### Resistivity Imaging

A pseudosection plot of the data [Fig. 14(a)] shows relatively smooth lateral variations with some evidence of 2D structures, especially in the first part of the profile. The model distance along the profile is 5 m and the lateral constraints were 0.12 for all model parameters. The 2D-LCI model of Fig. 14(b) identifies the same major units as the 2D smooth inversion of Fig. 14(c), but layer boundaries are more precisely identified (no a priori data were added). As seen by the drill log data superimposed on the model section, the agreement with the sand-clay boundaries is satisfying. The low-resistivity layer is thinner in the 2D-LCI than the smooth inversion model to the right of the profile. This is to be expected because the smooth inversion by nature smears out sharp structures. In the first half of the profile (0–500 m) steep 2D structures are indicated, whereas the structure in the last half of the profile is more 1D.

The 2D smooth inversion model [Fig. 14(c)] shows a smooth lateral and horizontal resistivity distribution with a high-resistivity top layer overlaying a low-resistivity layer. A high-resistivity structure is apparent in the bottom layer from approximately 450 to 1,000 m, but with a very uneven distribution. The 2D structures in the first half of the profile can also be tracked in the 2D smooth inversion model.

The groundwater level was not registered with the auger drillings and it is not possible to identify it clearly in any of the interpretations. For the right half of the profile, the groundwater level is possibly somewhere in the bottom layer below the clay layer. For the left half of the profile the model complexity makes it difficult to predict the groundwater level.

### Discussion

Both inverse models give good indications on the relative distribution of sandy and clayey materials. For the right half of the profile the 2D-LCI section identifies a relatively thin unit of clay in the upper part, no more than 6 m thick, which is confirmed by the drill log data at profile coordinate 500 m. In the 2D smooth inversion model the thickness of the low-resistivity body is hard

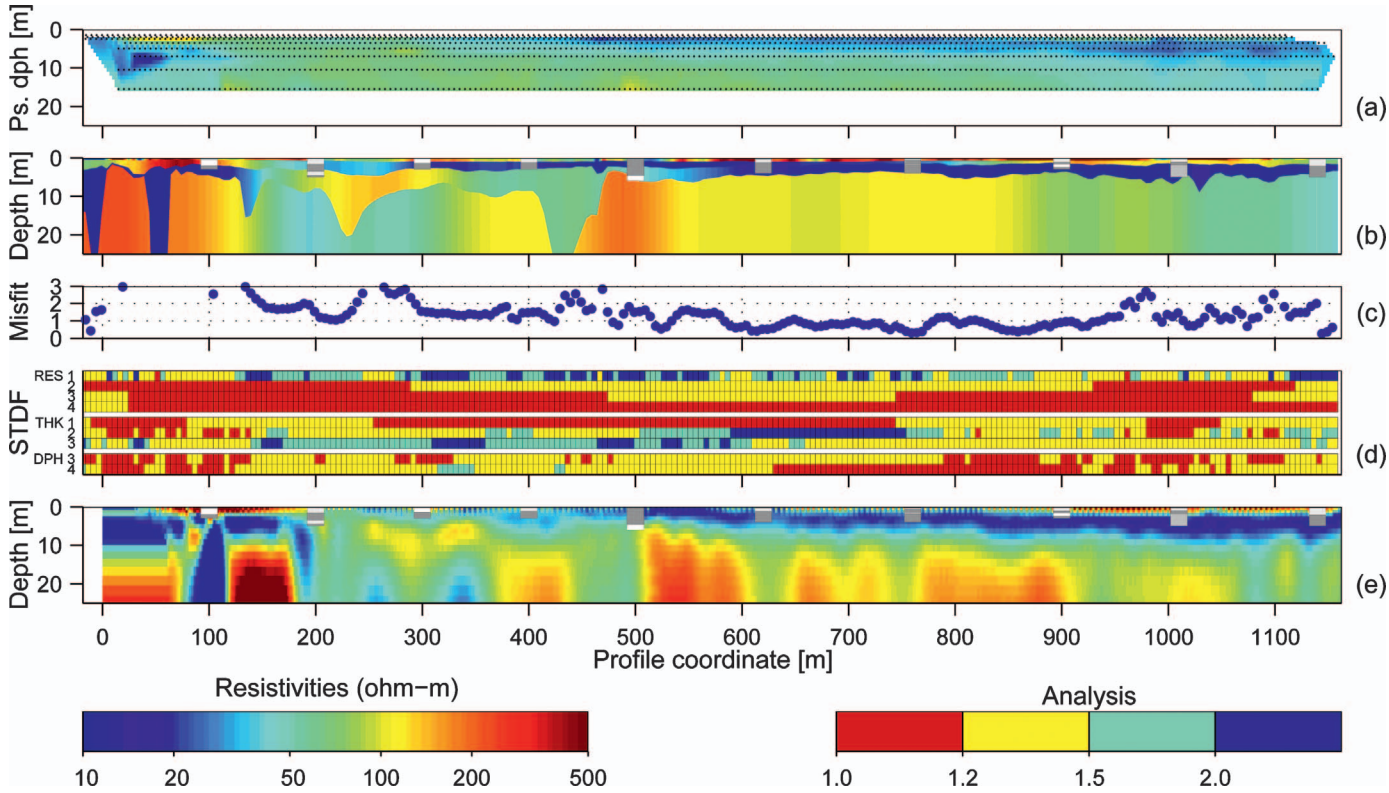


**Fig. 14.** (Color) (a) Apparent resistivity pseudosection for Case 3; (b) resulting 2D-LCI resistivity model with normalized residual errors [1 corresponding to error of 5% in (c) and standard deviation factors (STDF) of model parameters in (d)]; and (c) resistivity model from 2D smooth inversion. Sounding distance is 5 m. Data from shallow auger drilling are used to differentiate mainly between clay and clay rich till (dark grey) and various sands (light and white).

to identify, but most likely it is between 3 and 10 m. The cost difference associated with the removal of 3 m versus 10 m of clay is substantial, and the geotechnical challenges can be dramatically different; hence, a detailed description of unit thicknesses along the profiles is highly advantageous. A precise geophysical description enables a more accurate estimate of the total freeway construction costs.

## Conclusions

Successful mapping of significant features in geotechnical investigations is illustrated by the combination of 2D smooth inversion and 2D-LCI in the following three case histories:

1. In the railway trench construction case from southern Sweden a complex Quaternary geological environment is described in detail by the combination of 2D smooth inversion, 2D-LCI, and drill log data. This could not be accomplished using only one of the methods. The use of lithological information from geotechnical drill logs as a priori data in the 2D-LCI helps solve ambiguity in the inversion and increases confidence in the resistivity model.
2. In the slope stability case from Sweden the 2D-LCI, with refraction seismic results used as a priori data to constrain the inversion, solve equivalence problems in the resistivity model. The model parameter analysis clearly shows which parameters can be estimated and how the a priori data improves the final 2D-LCI resistivity model. This model constitutes a good basis for interpretation of all important geological units that can be used e.g., for stability calculations.
3. In the freeway construction case from Denmark a precise geophysical description enables a more accurate estimate of the total freeway construction costs, and to this the layered model from 2D-LCI contributes significantly.

Resistivity imaging is an important tool in many types of investigations, e.g., hydrogeology or geological hazard assessment, and it has been shown, here as well as by others, that it is also very useful in geotechnical site investigation. The 2D-LCI provides information that would not be possible to obtain with the 2D smooth inversion. In addition to looking at data misfit the model parameter analysis available from the LCI is an important tool for validation of the resistivity models. Simultaneous geological interpretation of resistivity models from the two methods affords good estimates of both layer boundaries and vertical features and the addition of a priori data in the 2D-LCI in the form of other types of data, such as drill log data or refraction seismic data, directly influences the resistivity models and subsequent interpretation.

## Acknowledgments

The writers would like to thank: Professor Leif Bjelm at the Department of Engineering Geology at Lund University, the City Tunnel Project, and Tyréns AB for providing an interesting case study and high-quality geotechnical and geological data; Rolf Larsson at the Swedish Geotechnical Institute for including the

Department of Engineering Geology at Lund University in the slope stability project; Björn Toresson at Impakt AB, who performed the refraction seismic measurements in Vagnhärad; the Danish Road Directorate, Ministry of Transport, for providing the highway construction data set; anonymous reviewers for making this paper accessible to a geo-engineering audience; and Louise Pellerin, Green Engineering, for her thoughtful review. NorFa granted a mobility scholarship to Roger Wisén to visit Aarhus University for 3 months during 2003. The Swedish Rescue Services Agency funded the slope stability study. Sven Tyréns foundation funded a large part of the Ph.D. studies of Roger Wisén.

## References

Auken, E., and Christiansen, A. V. (2004). "Layered and laterally constrained 2D inversion of resistivity data." *Geophysics*, 69, 752–761.

Bernstone, C., Dahlin, T., Ohlsson, T., and Hogland, W. (2000). "DC-resistivity mapping of internal landfill structures: Two pre-excavation surveys." *Environ. Geol.*, 39, 360–371.

Dahlin, T. (1993). "On the automation of 2D resistivity surveying for engineering and environmental applications." Doctoral thesis, Lund Univ., Lund, Sweden.

Dahlin, T. (1996). "2D resistivity surveying for environmental and engineering applications." *First Break*, 14, 275–283.

Dahlin, T. (2000). "Short note on electrode charge-up effects in DC resistivity data acquisition using multi electrode arrays." *Geophys. Prospect.*, 48, 181–187.

Dahlin, T. (2001). "The development of electrical imaging techniques." *Comput. Geosci.*, 27, 1019–1029.

Dahlin, T., Bjelm, L., and Svensson, C. (1999). "Use of electrical imaging in site investigations for a railway tunnel through the Hallandsås Horst, Sweden." *Q. J. Eng. Geol.*, 32, 163–172.

Dahlin, T., Leroux, V., and Nissen, J. (2002). "Measuring techniques in induced polarisation imaging." *J. Appl. Geophysics*, 50, 279–298.

Danish Geotechnical Institute. (1999). "Boring campaign 1998, Geological model." *Rep. No.*, *1*, *prepared for the City Tunnel Project (CTP) in Malmö, Sweden*, Lyngby, Denmark.

Griffiths, D. H., and Barker, R. D. (1993). "Two-dimensional resistivity imaging and modeling in areas of complex geology." *J. Appl. Geophysics*, 29, 211–226.

Griffiths, D. H., and Turnbull, J. (1985). "A multi-electrode array for resistivity surveying." *First Break*, 3, 16–20.

Hack, R. (2000). "Geophysics for slope stability." *Surv. Geophys.*, 21, 423–448.

Hiltunen, D. R., and Roth, M. J. S. (2004). "Investigation of bridge foundation sites in karst terrane via multi-electrode electrical resistivity." *Geotechnical and geophysical site characterization*, A. Viana da Fonseca and P. W. Mayne, eds., Millpress, Rotterdam, 483–489.

Jackson, D. D. (1979). "The use of a priori data to resolve nonuniqueness in linear inversion." *Geophys. J. R. Astron. Soc.*, 57, 137–157.

Johansen, H. K. (1977). "A man/computer interpretation system for resistivity soundings over a horizontally stratified earth." *Geophys. Prospect.*, 25, 667–691.

Larsen, F., Owen, R., Dahlin, T., Mangeya, P., and Barmen, G. (2002). "A preliminary analysis of the groundwater recharge to the Karoo formations, mid-Zambezi basin, Zimbabwe." *Phys. Chem. Earth, Part B*, 27, 765–772.

Loke, M. H., and Barker, R. D. (1996). "Rapid least-squares inversion of apparent resistivity pseudosections by quasi-Newton method." *Geophys. Prospect.*, 44, 131–152.

Marquart, D. (1963). "An algorithm for least squares estimation of nonlinear parameters." *J. Appl. Math.*, 11, 431–441.

McGrath, R. J., Styles, P., Thomas, E., and Neale, S. (2002). "Integrated high-resolution geophysical investigations as potential tools for water resource investigations in karst terrain." *Environ. Geol.*, 42, 552–557.

Morgenstern, N. R. (2000). *Proc., Common Ground: GEOENG 2000: An Int. Conf. Geotechnical and Geological Engineering*, Technomic Publishing, Melbourne, 1–20.

Oldenburg, D. W., and Li, Y. (1994). "Inversion of induced polarization data." *Geophysics*, 59, 1327–1341.

Parasnis, D. S. (1997). *Principles of applied geophysics*, 5th Ed., Chapman & Hall, London.

Pellerin, L. (2002). "Applications of electrical and electromagnetic methods for environmental and geotechnical investigations." *Surv. Geophys.*, 23, 101–132.

Sharp, J. C., Kaiser, P. K., Diedrichs, M. S., Martin, C. D., and Steiner, W. (2000). "Underground works in hard rock tunnelling and mining." *Proc., GEOENG 2000: An Int. Conf. Geotechnical and Geological Engineering*, Technomic, Melbourne, 841–926.

Sørensen, K. I. (1996). "Pulled array continuous electrical profiling." *First break*, 14, 85–90.

Sørensen, K. I., Auken, E., Christensen, N. B., and Pellerin, L. (2005). "An integrated approach for hydrogeophysical investigations: New technologies and a case history." *Near-surface geophysics*, Part II, 585–603, SEG. Book Chapter.

Stokoe, K. H., Joh, S. H., and Woods, R. D. (2004). "The contribution of in situ geophysical measurements to solving geotechnical engineering problems." *Geotechnical and geophysical site characterization*, A. Viana da Fonseca and P. W. Mayne, eds., Millpress, Rotterdam, 97–132.

Suzuki, K., Toda, S., Kusunoki, K., Fujimitsu, Y., Mogi, T., and Jomori, A. (2000). "Case studies of electrical and electromagnetic methods applied to mapping active faults beneath the thick quaternary." *Eng. Geol. (Amsterdam)*, 56, 29–45.

Tarantola, A., and Valette, B. (1982). "Generalized nonlinear inverse problems solved using a least squares criterion." *Rev. Geophys.*, 20, 219–232.

van Overmeeren, R. A., and Ritsema, I. L. (1988). "Continuous vertical electrical sounding." *First Break*, 6, 313–324.

Ward, S. H., and Hohmann, G. W. (1987). "Electromagnetic theory for geophysical applications." *Electromagnetic methods in applied geophysics*, M. N. Nabighian, ed., Society of Exploration Geophysics, 285–426.

Wisén, R., Auken, E., and Dahlin, T. (2005). "Combination of 1D laterally constrained inversion and 2D smooth inversion of resistivity data with a priori data from boreholes." *Near Surface Geophysics*, 3, 71–79.

Zhou, B., and Dahlin, T. (2003). "Properties and effects of measurement errors on 2D resistivity imaging surveying." *Near Surface Geophysics*, 1, 105–117.